coatings

MDPI

Article

The Impact of Bias and Nitrogen Pressure on TiNbN Coatings in Arc-PVD Processes—A Multifactorial Study

Henry Dempwolf [1,*], Matthias Proft [1], Axel Baumann [1], Sinah Malz [2] and Olaf Keßler [2]

[1] DOT GmbH, Charles Darwin-Ring 1a, D-18059 Rostock, Germany; maprojekt@hotmail.de (M.P.); baumann@dot-coating.de (A.B.)
[2] Faculty of Mechanical Engineering and Marine Technology, Chair of Materials Science, University of Rostock, Justus-von-Liebig-Weg 2, D-18059 Rostock, Germany; sinah.malz@uni-rostock.de (S.M.); olaf.kessler@uni-rostock.de (O.K.)
* Correspondence: dempwolf@dot-coating.de

Abstract: Titanium-based nitride physical vapour deposition (PVD) coatings, such as titanium nitride (TiN), are state-of-the-art solutions for surface modifications of CoCrMo-based implants for patients who are hypersensitive to metallic ions such as cobalt, chromium and nickel. Variations of the process parameters during the cathodic arc evaporation are known to exhibit an impact on the surface properties of coatings. The aim of this study was to characterise the effect of the substrate bias and the nitrogen pressure on the surface properties of TiNbN coatings deposited on CoCrMo alloys in a limited parameter set. Eighteen parameter sets were coated with TiNbN. The substrate bias (−100 to −200 V) and the nitrogen pressure (0.3–3.0 Pa) were selected following a randomised, multifactorial response surface test design. The coating thickness, roughness, hardness and scratch resistance were measured following standardised procedures. The structure of the coating was analysed by SEM and XRD. The substrate bias and the pressure exhibited a significant impact on the coating thickness and the surface roughness. The grain growth was predominantly impacted by the bias. The parameter variation did not show any significant impact on the XRD, hardness or scratch test results.

Keywords: titanium niobium nitride (TiNbN); physical vapour deposition (PVD); cathodic arc evaporation; substrate bias; nitrogen pressure; coating thickness; roughness; response surface model

Citation: Dempwolf, H.; Proft, M.; Baumann, A.; Malz, S.; Keßler, O. The Impact of Bias and Nitrogen Pressure on TiNbN Coatings in Arc-PVD Processes—A Multifactorial Study. *Coatings* **2022**, *12*, 935. https://doi.org/10.3390/coatings12070935

Academic Editor: Christian Mitterer

Received: 1 May 2022
Accepted: 28 June 2022
Published: 1 July 2022

1. Introduction

Titanium nitride (TiN) coatings are an established surface treatment for metallic implants [1]. TiN is applied to CoCrMo alloys to reduce the allergic potential of metallic ions to the surrounding tissue [2] and to minimise the abrasive wear of metallic hip [3] and knee components [4]. Due to a more ductile substrate material, physical vapour deposition (PVD)-coated implant components show a reduced risk of breakage compared to ceramic implants [5]. Furthermore, PVD-coated implant surfaces exhibit ceramic surface characteristics, such as a high wettability [3], an improved surface hardness [6,7] and an enhanced tribological performance in vitro [4,6] and ex vivo [3,8]. Consequently, PVD-coated metal implants exhibit superior clinical data [1,9].

TiN coatings have been state of the art for the surface treatment of orthopaedic and dental implants for many decades. However, comparatively new hard PVD coatings, such as TiAlN, ZrN and TiNbN, are advancing in the medical industry [9–12]. The application of TiNbN coatings instead of TiN coatings is described in the literature, and for the same reasons: the reduction in metallic ion diffusion and abrasive wear of articulating implant surfaces [9,10,13]. Therefore, TiNbN is commonly applied by cathodic arc PVD processes.

The process parameters are known to have a significant impact on the properties of hard PVD coatings, particularly the reactive gas atmospheres' influence on the evaporation in arc processes by forming compound layers on PVD target surfaces [14]. The change in

arc spot behaviour in relation to the gaseous atmosphere was analysed by Oh et al. [15,16], indicating a more enhanced spot movement at higher gas pressures.

The impact of the coating parameters (such as nitrogen pressure and substrate temperature) on the structure of sputtered films are adequately described by the structure zone models (SZM) of Thornton [17–19]. Messier et al. [20] introduced the surface mobility of adatoms as a factor that impacts the surface structure. Furthermore, variations in the coating process show a significant impact on the coating morphology [21,22] and the mechanical characteristics, such as hardness and scratch resistance [23,24]. Anders [25] proposed a revised SZM, taking the generalised temperature into account for the potential and normalised energy of the kinetic energy of particles arriving at the substrate surface. This revised SZM also qualitatively describes the impact of the potential and kinetic energy of the particles on the film thickness.

However, despite some clinical data on the outcome of TiNbN-coated implants of Herbster et al. [8] and Bergschmidt et al. [13], and the biocompatibility [26,27] and wear performance of TiNbN in vitro [10,12] and ex vivo [4,8], there are no published studies on the basic mechanical properties and structure of TiNbN coated by cathodic arc processes.

Cicek et al. [28] performed a comparative study of reactively sputtered films, including TiNbN on steel substrates. However, these findings did not describe significant results for clinical applications because the coatings studied were thin (<0.5 µm) in comparison to coatings with clinical relevance as described by Fabry et al. [3,4] and Herbster et al. [8]. Additionally, there is no reactively magnetron-sputtered TiNbN coating in common clinical use in orthopaedic implants.

In general, the impact of the process parameters during the PVD process on the mechanical properties and the structure of TiNbN is not characterised in the literature. In this work, we present a parameter study of TiNbN applied via a cathodic arc process. The objective of this study was to characterise the impact of the negative substrate bias and the nitrogen pressure on the structural and the mechanical properties of TiNbN coatings in a limited parameter set. The surface properties were described by a mathematical model based on the response surface method, which is commonly used in the design of experimental approaches [29]. The aim of this study was to generate a fundamental understanding of the dominant process factors of medical cathodic arc TiNbN coatings.

2. Materials and Methods

2.1. Sample Preparation and Layer Deposition

All of the samples in this study (coupons of 25 mm diameter and 8 mm height) were manufactured from medical grade CoCrMo alloy, in accordance with DIN ISO 5832-12 [30]. The chemical composition of the alloy used in this study is listed in Table 1. The surfaces of the samples were ground and mirror polished to Ra < 0.01 µm and cleaned in an alkaline ultrasound bath prior to coating.

Table 1. Chemical composition of the CoCrMo alloy.

Element	wt %
Cobalt (Co)	Balance
Chromium (Cr)	27.50
Molybdenum	5.50
Iron (Fe)	0.31
Manganese (Mn)	0.81
Nickel (Ni)	0.11
Silicon (Si)	0.62
Carbon (C)	0.04

Coatings were applied in the production process of the DOT GmbH (Rostock, Germany) using a Vacotec Alpha 400 coating chamber. The surface of the samples was conditioned using sputter cleaning processes. Before establishing the nitrogen atmosphere for the TiNbN coating, a TiNb layer with a coating thickness <0.1 µm was deposited as part

of the surface preparation, in constant conditions for all samples (Bias −100 V, Pressure 0.3 Pa, Ar atmosphere). Subsequently, the coating was applied. During the coating process, the processing time (40 min), substrate temperature (400 °C), arc current (65 A) and the target configuration (5 equal targets) were kept constant. All sample batches were coated using arc targets with a composition 70 wt % Ti and 30 wt % Nb. The TiNbN coating was formed under a reactive nitrogen atmosphere.

The bias and the nitrogen pressure of the coating process were varied, following a multifactorial equidistant study design with six levels of bias (−100 V, −120 V, −140 V, −160 V, −180 V, and −200 V) and three levels of nitrogen pressure (0.3 Pa, 1.7 Pa, and 3.0 Pa), resulting in 18 parameter sets. The parameter sets were designed to generate a sample plan within the field of common technical applications of arc-processed TiNbN surfaces. The bias was varied within small boundaries to show a good resolution of the effect on the coating properties in the results. The sampling plan and the running order of the parameter sets were randomised to minimise inherent process effects.

Prior to the testing, the samples were cleaned in an alkaline solution, rinsed with de-ionised water and dried under vacuum conditions (this surface configuration is referred to as 'as coated' in this study).

Finally, the samples were post-processed to remove residues of the arc process. Therefore, the samples were manually lapped with an abrasive fleece. The cleaning process was repeated after the lapping process (this surface configuration is referred to as 'finished' in this study).

2.2. Coating Thickness, Structure and Morphology Analysis

The coating thickness was determined in accordance with DIN EN ISO 26,423 [31] for flat surfaces. An abrasion testing device (kaloMax NT II—BAQ GmbH, Braunschweig, Germany), a 20 mm hardened steel ball (100Cr6) and a diamond suspension (Calotest-hq, Eifeler Suedcoating GmbH, Ettlingen, Germany) were used to prepare the samples. Subsequently, each grinding was analysed by calculating the coating thickness with the inner diameter and the outer diameter of the visible coating on the crater grinding. The results were obtained with an accuracy of 0.1 µm. At least three measurements were performed per parameter set.

Roughness measurements of coated samples were performed for one dimensional line roughness parameters and for two dimensional surface roughness parameters. All of the tests were conducted using a confocal laser scanning microscope (LEXT OLS 4000, Olympus, Tokyo, Japan).

The arithmetic mean height (R_a), the maximum height of the profile (R_z), the mean peak height (R_p) and the mean valley depth (R_v) were measured to characterise the line roughness of the coated samples. The line roughness was determined in accordance with ISO standards [32,33] using a cut off length of λ_c = 0.25 mm and a total measurement length of 1.25 mm. A 20x objective with a working distance of 1.0 mm and a numeric aperture of 0.6 was applied for all line roughness measurements.

The surface roughness was measured using a 50x objective with a working distance of 0.35 mm and a numeric aperture of 0.95. All measurements of the surface roughness were performed on image sizes of 0.25 mm × 0.25 mm, with a cut off length of λ_c = 0.25 mm. Surface roughness measurements were performed for the most significant roughness parameters for tribological applications, i.e., the arithmetic mean roughness (S_a), the maximum height (S_z), the reduced peak height (S_{pk}) and the reduced valley depth (S_{vk}) [34].

Finally, the roughness measurements were repeated after a post-processing step, to compare surfaces as coated and finished for applications on endoprostheses. Roughness measurements were performed on three different samples per parameter set, with five repetitions per sample, resulting in 15 single measurements per parameter set.

The structure of the TiNbN coating in different parameter sets was described via SEM analysis. For this purpose, the coatings were applied to foils of austenitic stainless steel (X5CrNi18-10) in the same PVD batch as the CoCrMo samples. The PVD coating structure is

assumed to be similar on CoCrMo substrates. Subsequently, the samples were prepared by breaking the foils manually. The fractured surfaces were analysed under the SEM. The SEM images were used to qualitatively specify the structure of the TiNbN samples in accordance with existing structure models.

X-ray diffraction diagrams of TiNbN coatings were recorded on a Bruker D8 Discover diffractometer with Cu-Kα radiation (wave length 0.1541 nm). The 2θ diffraction angles from 20° to 120° were analysed by a VANTEC-1 line-detector. Sample tilt angle was set to $\psi = 0°$. Diffraction peaks were compared to reference data for cubic TiN with a lattice spacing of 0.4241 nm from the Crystallography Open Database [35], using MATCH! software [36].

2.3. Mechanical Properties Testing

The hardness of the TiNbN samples was determined using the instrumented indentation tests, in accordance with DIN EN ISO 14577-4 [37]. All tests were performed using a Fischerscope HM2000 (Helmut Fischer, Sindelfingen, Germany) with a Vickers Diamond. The maximum load was limited to 80 mN to ensure a maximum indentation depth of 10% of the coating thickness for all samples. Hardness measurements were performed on three different samples per parameter set, with ten repetitions per sample, resulting in 30 single measurements per parameter set.

All parameter sets underwent scratch tests, in accordance with DIN EN ISO 20502 [38]. The maximum load was limited to 100 N. The load was continuously increased at a rate of 198 N/min over a test distance of 5 mm, using a Rockwell C diamond with a tip radius of 200 µm. The critical loads for the formation of cracks (Lc1), delamination (Lc2) and exhaustion (Lc3) were determined on five samples per parameter set.

2.4. Numerical Analysis and Statistical Methods

All test result plots were illustrated as mean ± standard deviation. The coating characteristics (coating thickness, roughness, hardness, and scratch resistance) were presented as a function of the bias and the pressure.

Furthermore, the impact of both process parameters on the coating properties was evaluated using the response surface method (RSM) to generate a mathematical meta-model of the coating process. Therefore, a process was evaluated at multiple points and the meta-model was approximated by a least square fit regression [29].

The response surface was obtained by taking all single measurements of the coating characteristics (coating thickness, roughness, hardness, and scratch resistance) inside the parameter set (bias −100 to −200 V, pressure 0.3–3.0 Pa) into account. The model of the response surface was limited to a polynomial regression of the second order. All calculations were performed with the RSM package of the R-language [29,39].

The mathematical centre point of the response surface was set at a bias of −150 V and a pressure of 1.65 Pa. The increment of the RSM was adjusted to 20 V and 1.35 Pa for the bias and the pressure, respectively. All variables (bias and pressure) were normalised in accordance with the RSM package [39]. The mathematical regression model resulted in a quadratic equation (Equation (1)) which is described by six coefficients, where x_1 equals the bias and x_2 equals the nitrogen pressure.

$$y = c_1 + c_2x_1 + c_3x_2 + c_4x_1x_2 + c_5x_1^2 + c_6x_2^2 \quad (1)$$

The coefficients of the quadratic equation were calculated using the functionality of the RSM package. Furthermore, a t-test was performed on the impact of the linear factors, the quadratic proportion of the factors and the interaction of bias and pressure on the characteristics of the coating. A probability value $p < 0.05$ was considered significant within this study.

Finally, the contour plots of the response surface of the coating characteristics (such as coating thickness and roughness) were plotted as a function of the bias and the nitrogen pressure using the RSM package.

3. Results

3.1. Coating Thickness

As shown in Figure 1, the coating thickness increases with increased nitrogen pressure, from about 4.5 µm at 0.3 Pa, to 7.5 µm at 3.0 Pa. Furthermore, the increase in the negative bias results in a slight decrease in the resulting coating thickness. The results of the statistical analysis show a significant impact of the pressure ($p < 0.001$) and bias ($p = 0.002$) on the coating thickness. The pressure also exhibits a significant quadratic proportion ($p < 0.001$).

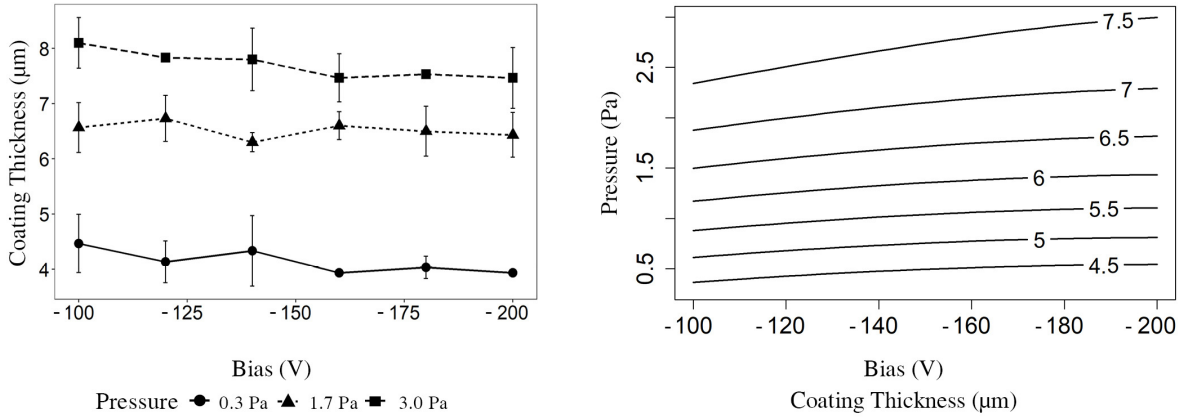

Coefficient	Bias	Pressure	Interaction of Bias & Pressure	$Bias^2$	$Pressure^2$
p-value	0.002 (*)	3.16×10^{-14} (*)	0.601	0.352	1.29×10^{-5} (*)
*indicates statistical significance					

Figure 1. Scatter plot and response surface of the coating thickness.

3.2. Roughness

The line roughness (R_a and R_z) exhibits a maximum at the lowest pressure (0.3 Pa) and decreases with an increase in the PVD processing pressure (Figures 2 and 3). This effect is significant for the line roughness parameters. The tables of Figures 2 and 3 display a p value of 0.001 for as coated samples. Finished samples exhibit an even more significant impact of the processing pressure.

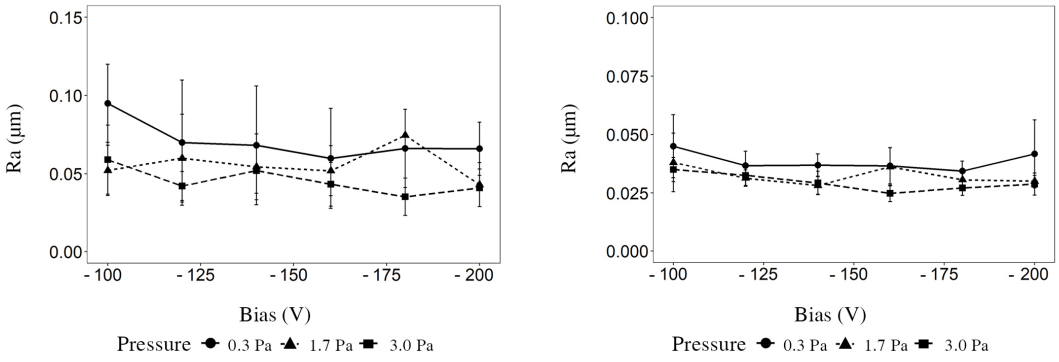

Figure 2. *Cont.*

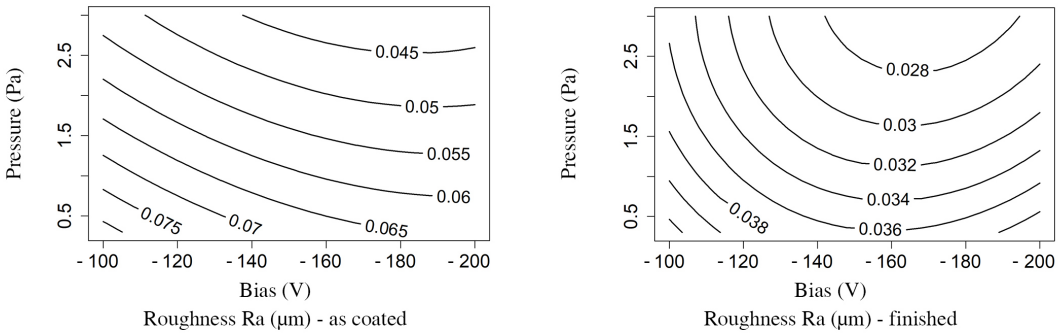

Coefficient	Bias	Pressure	Interaction of Bias & Pressure	Bias^2	Pressure^2
p-value as coated	0.072	0.001 (*)	0.692	0.488	0.746
p-value finished	0.017 (*)	9.52 x 10^{-5} (*)	0.402	0.009 (*)	0.286
*indicates statistical significance					

Figure 2. Scatter plots and response surface of the line roughness Ra as coated and finished.

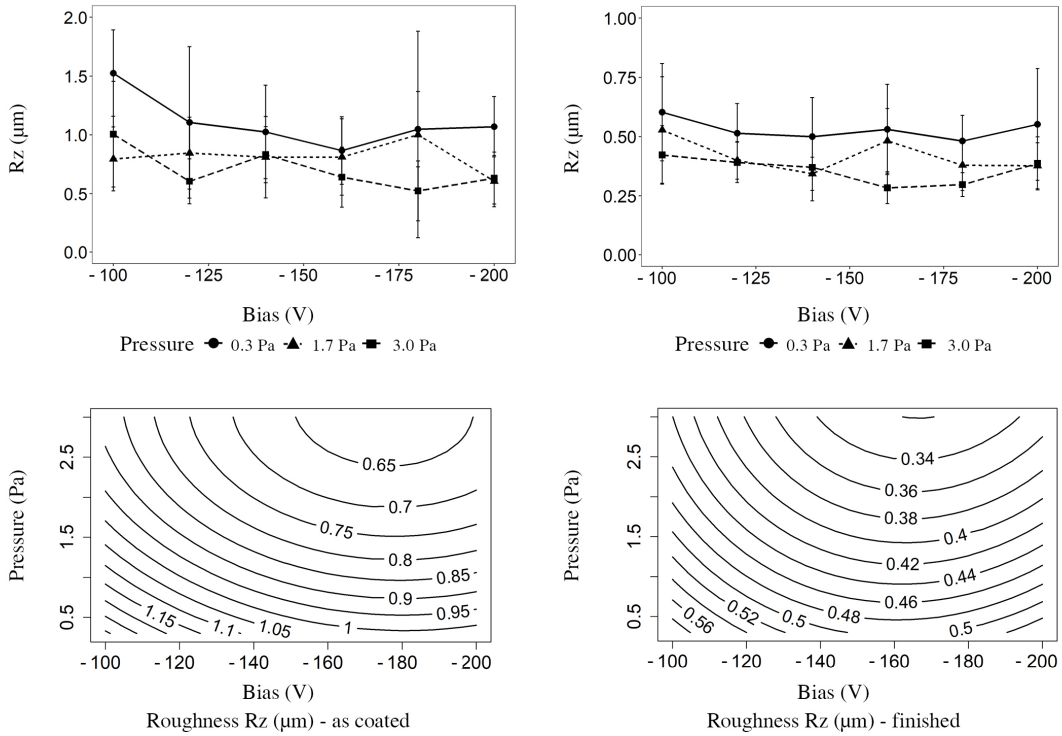

Coefficient	Bias	Pressure	Interaction of Bias & Pressure	Bias^2	Pressure^2
p-value as coated	0.038 (*)	0.001 (*)	0.853	0.246	0.293
p-value finished	0.037 (*)	2.82 x 10^{-5} (*)	0.677	0.255	0.332
*indicates statistical significance					

Figure 3. Scatter plots and response surface of the line roughness Rz as coated and finished.

Furthermore, an increase in the negative bias shows a significant reduction in the line roughness. Consequently, R_a and R_z exhibit a local minimum at 3.0 Pa chamber pressure, and a bias of −180 V for unfinished samples and −160 V for samples after finishing, respectively. The finishing process after the PVD coating resulted in a reduction in all roughness parameters.

The effect of the finishing process is significant, with respect to the peak height of the roughness profile (R_p). The maximum R_p of unfinished samples is 0.8 µm (Figure 4) while the maximum R_p of finished samples is below 0.25 µm. The maximum valley depth is also significantly reduced. All samples show R_v below 0.5 µm after the finishing process (Figure 5).

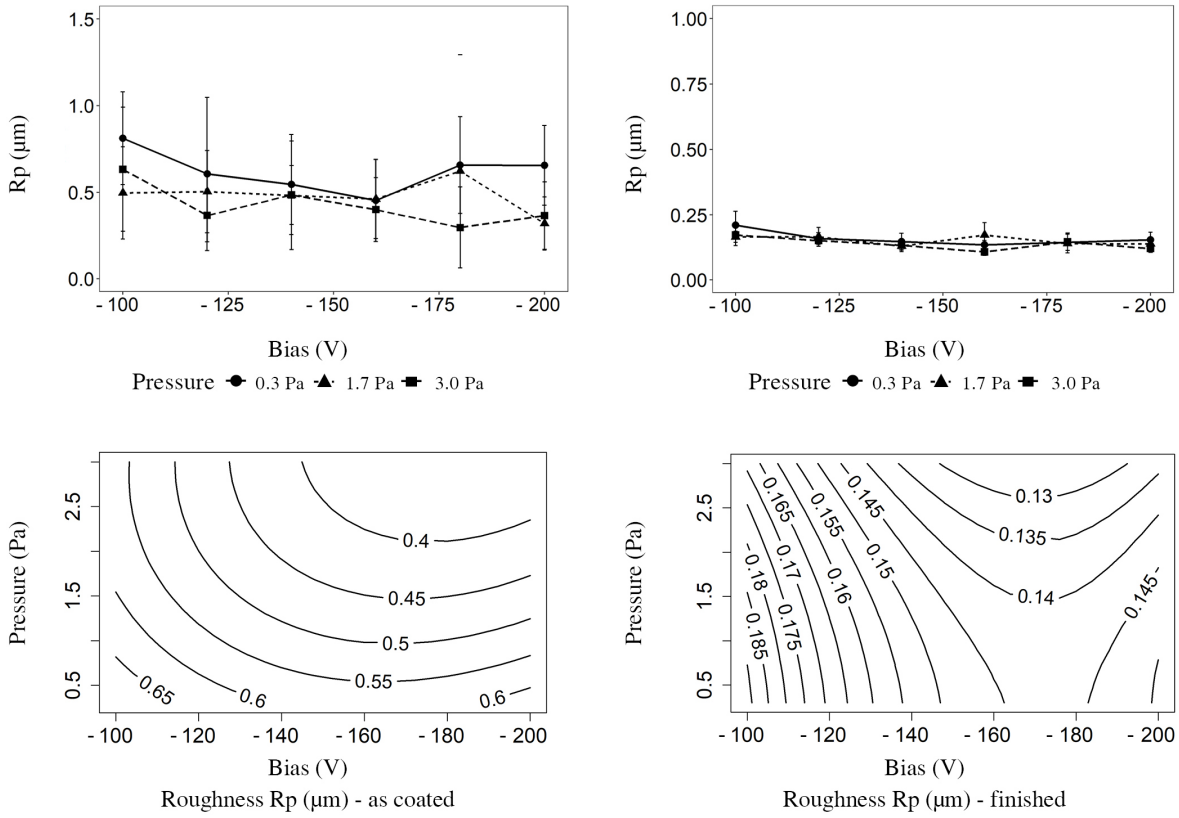

Coefficient	Bias	Pressure	Interaction of Bias & Pressure	Bias²	Pressure²
p-value as coated	0.079	0.006 (*)	0.478	0.234	0.478
p-value finished	0.006 (*)	0.062	0.849	0.042 (*)	0.641
*indicates statistical significance					

Figure 4. Scatter plots and response surface of the line roughness Rp as coated and finished.

Furthermore, the process pressure shows a significant impact ($p = 0.006$) on R_p, resulting in a reduction in the peak height when increasing the nitrogen pressure. The process pressure exhibits the same effect on the maximum valley depth (R_v) with $p < 0.001$ for as coated and finished samples, respectively.

The negative substrate bias ($p = 0.006$) and the quadratic proportion ($p = 0.042$) of the bias exhibit a significant impact on the maximum peak height (R_p), resulting in a local minimum at −160 to −180 V.

The surface roughness values S_a and S_z exhibit a local minimum at a substrate bias of −160 V for all pressures (Figure 6). Accordingly, in the table of Figure 6, the RSM analysis shows a significant impact of the substrate bias or the quadratic proportion of the bias on all surface roughness parameters, while the pressure does not exhibit a significant impact on the surface roughness.

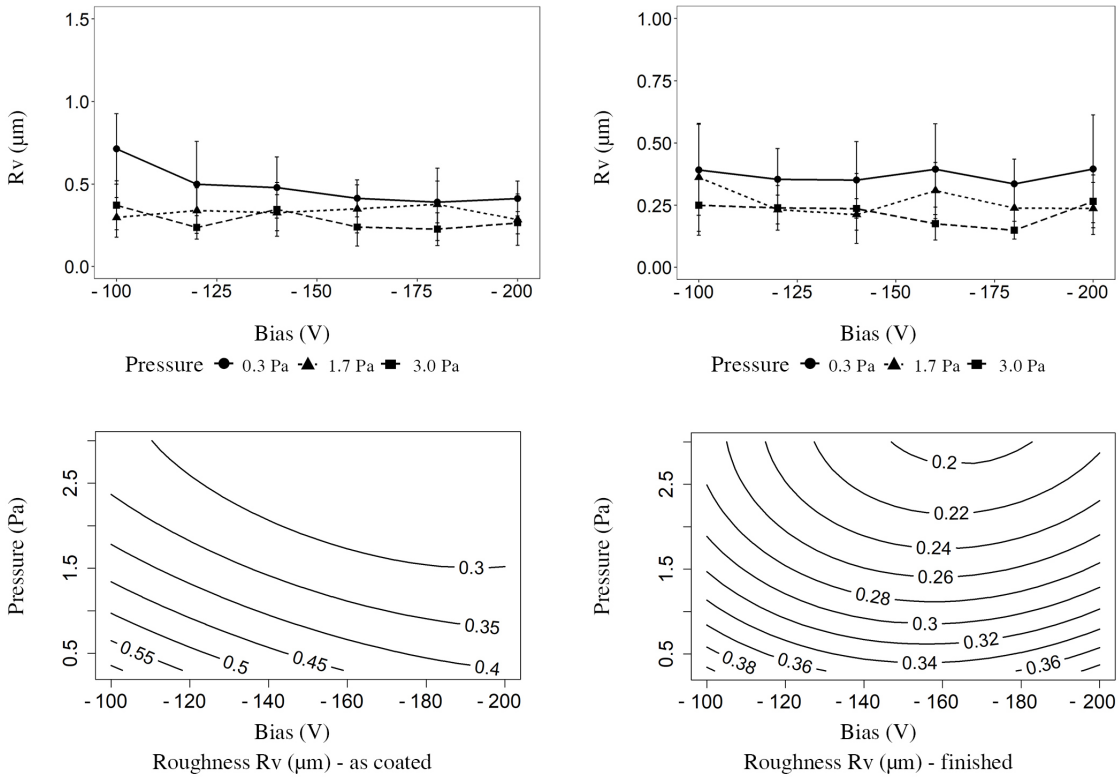

Coefficient	Bias	Pressure	Interaction of Bias & Pressure	Bias^2	Pressure^2
p-value as coated	0.021 (*)	0.000 (*)	0.131	0.343	0.153
p-value finished	0.243	4.43 x 10^{-5} (*)	0.601	0.089	0.226
*indicates statistical significance					

Figure 5. Scatter plots and response surface of the line roughness Rv as coated and finished.

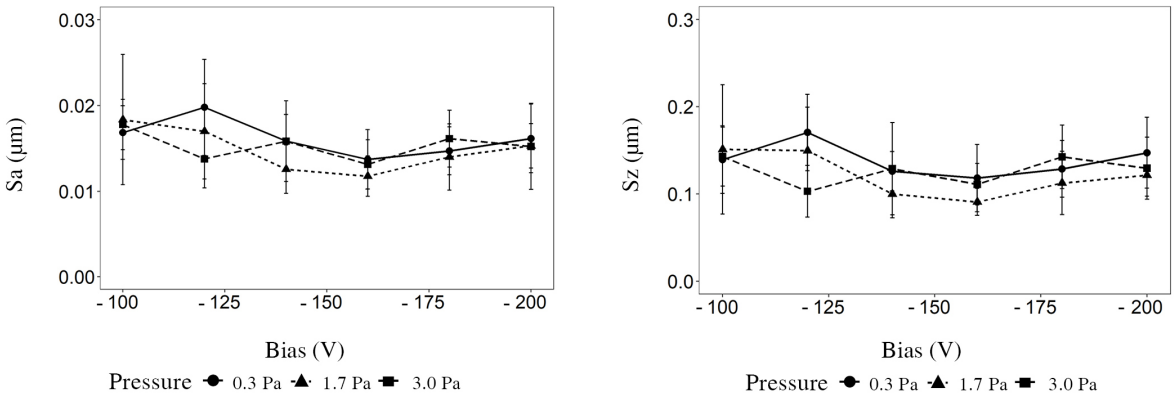

Figure 6. *Cont.*

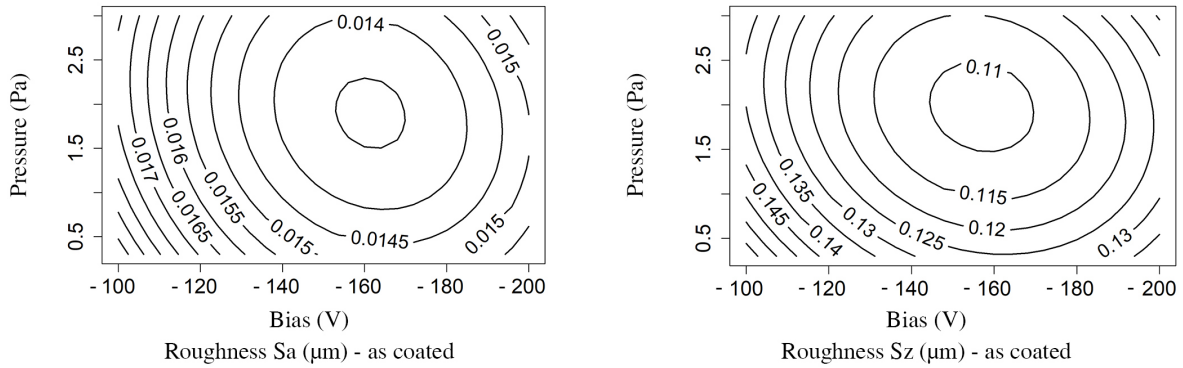

Coefficient	Bias	Pressure	Interaction of Bias & Pressure	Bias^2	Pressure^2
p-value Sa	0.044 (*)	0.389	0.549	0.019 (*)	0.300
p-value Sz	0.234	0.274	0.583	0.043 (*)	0.242
*indicates statistical significance					

Figure 6. Scatter plot and response surface of surface roughness Sa and Sz (as coated).

The mean peak height S_{pk} also exhibits a local minimum of 0.009 µm–0.016 µm at a bias of −160 V for all pressures in this test series (Figure 7). S_{vk} shows a minimum at −180 V. The quadratic proportion of the substrate bias presents a significant processing factor for S_{pk} and S_{vk} in the table of Figure 7.

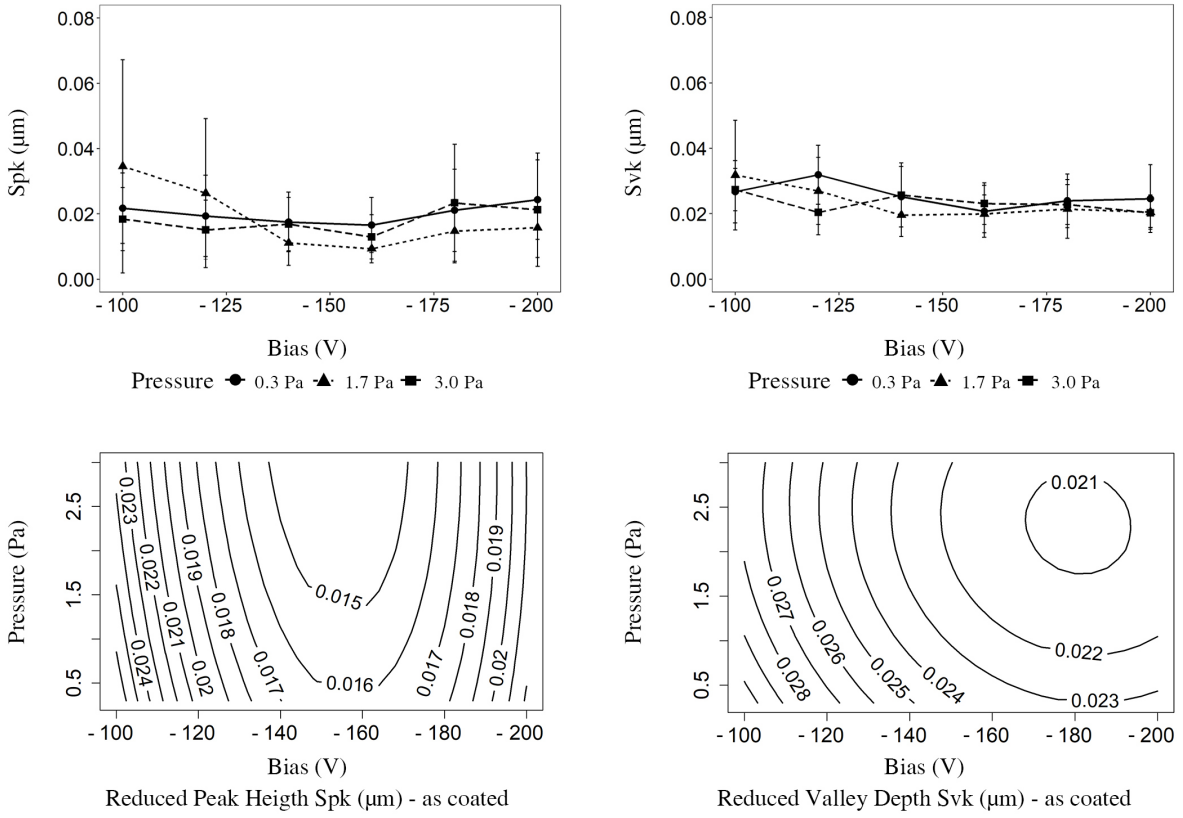

Figure 7. *Cont.*

Coefficient	Bias	Pressure	Interaction of Bias & Pressure	Bias^2	Pressure^2
p-value Spk	0.350	0.520	0.835	0.026 (*)	0.899
p-value Svk	0.008 (*)	0.230	0.854	0.017 (*)	0.533
*indicates statistical significance					

Figure 7. Scatter plot and response surface of surface roughness Spk and Svk (as coated).

The finishing process leads to a significant reduction in S_a and S_z, exhibiting a maximum below 0.015 µm and 0.120 µm, respectively (Figure 8). The finishing process also leads to a significant reduction in S_{pk}, with a global maximum of 0.12 µm. S_{vk} is less affected by the finishing process (Figure 8).

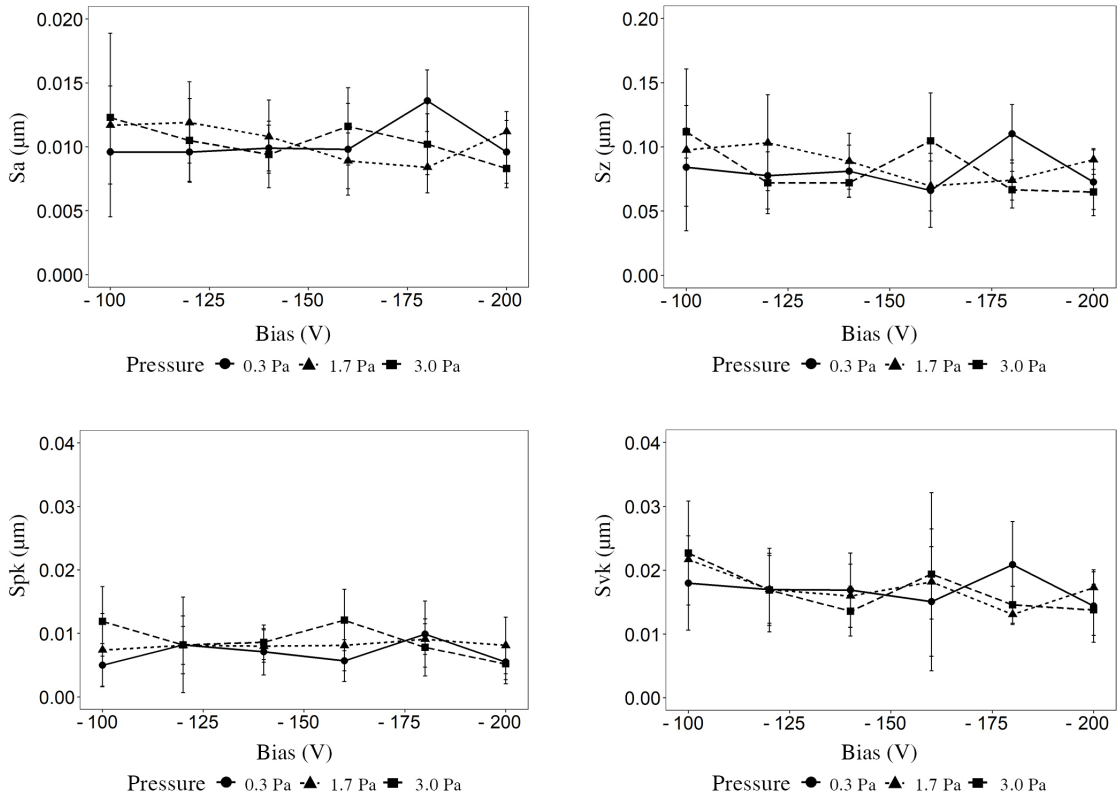

Coefficient	Bias	Pressure	Interaction of Bias & Pressure	Bias^2	Pressure^2
Sa	0.201	1.000	0.922	0.564	0.420
Sz	0.204	0.824	0.663	0.444	0.934
Spk	0.880	0.472	0.934	0.624	0.388
Svk	0.158	0.482	0.474	0.629	0.789
*indicates statistical significance					

Figure 8. Scatter plot of surface roughness Sa, Sz, Spk and Svk (finished).

The table of the RSM analysis reveals no significant impact on the process parameters on the surface roughness after the finishing process.

3.3. SEM

The SEM analysis shows a qualitative difference in the coatings applied at a bias of −100 V (Figure 9a at 3.0 Pa and Figure 9c at 0.3 Pa) and −200 V (Figure 9b at 3.0 Pa and Figure 9d at 0.3 Pa). The TiNbN layers show a more columnar structure at a bias of −200 V, compared to lower negative bias parameters. The columns at a higher negative bias show a continuous growth from the substrate interface to the top layer of the coating.

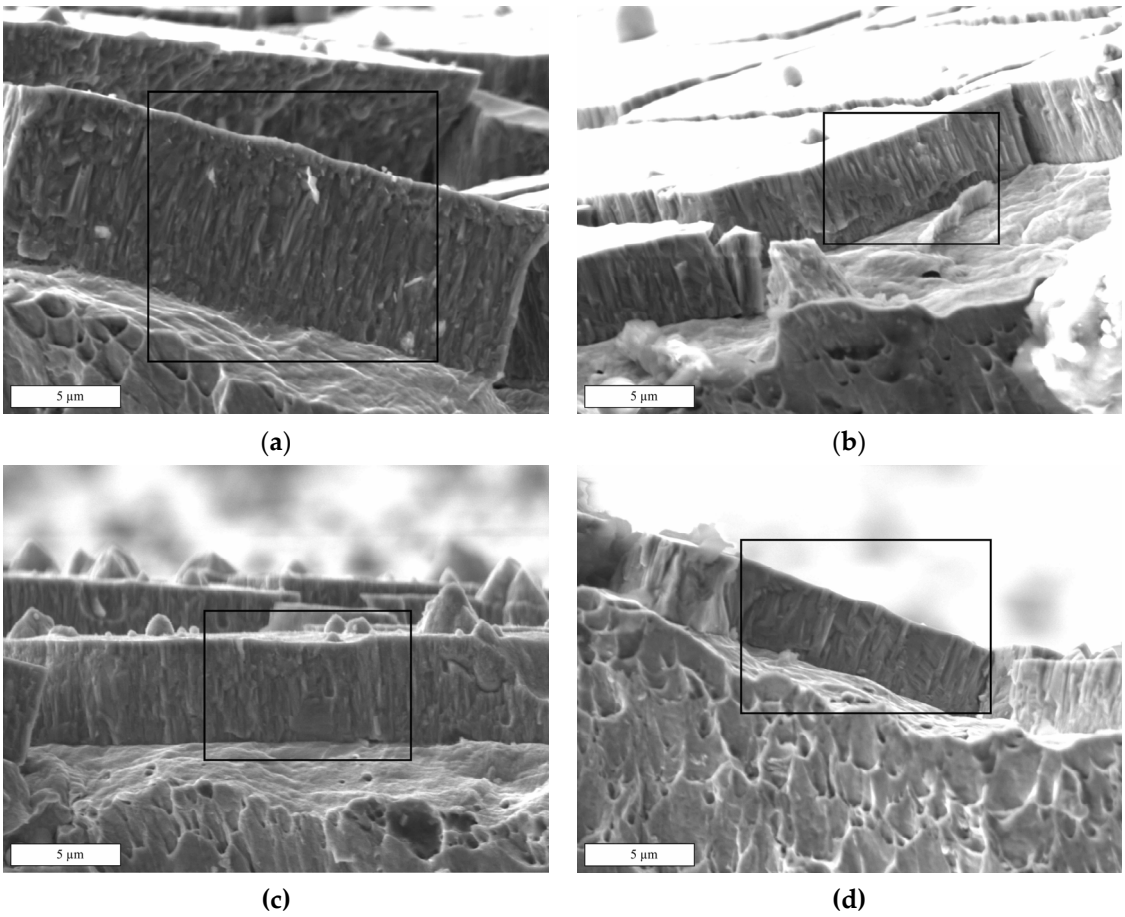

(**a**) (**b**)

(**c**) (**d**)

Figure 9. SEM Images of TiNbN at (**a**) 3 Pa and −100 V, (**b**) 3 Pa and −200 V, (**c**) 0.3 Pa and −100 V, and (**d**) 0.3 Pa and −200 V; region of interest is specified by boxes.

3.4. XRD Analysis

Figure 10 shows XRD diagrams of five TiNbN variants in the centre and the corners of the pressure/bias parameter field. All diffraction patterns look very similar and agree with the cubic TiN crystal structure. The sole appearance of {111} and {222} diffraction peaks hint at a {111} fibre texture in the coating perpendicular to the substrate surface. Furthermore, all peak positions are shifted to lower 2θ angles than the reference of TiN. Besides the influence of the Nb content on the lattice spacing, this shift hints at compressive residual stresses in the coating.

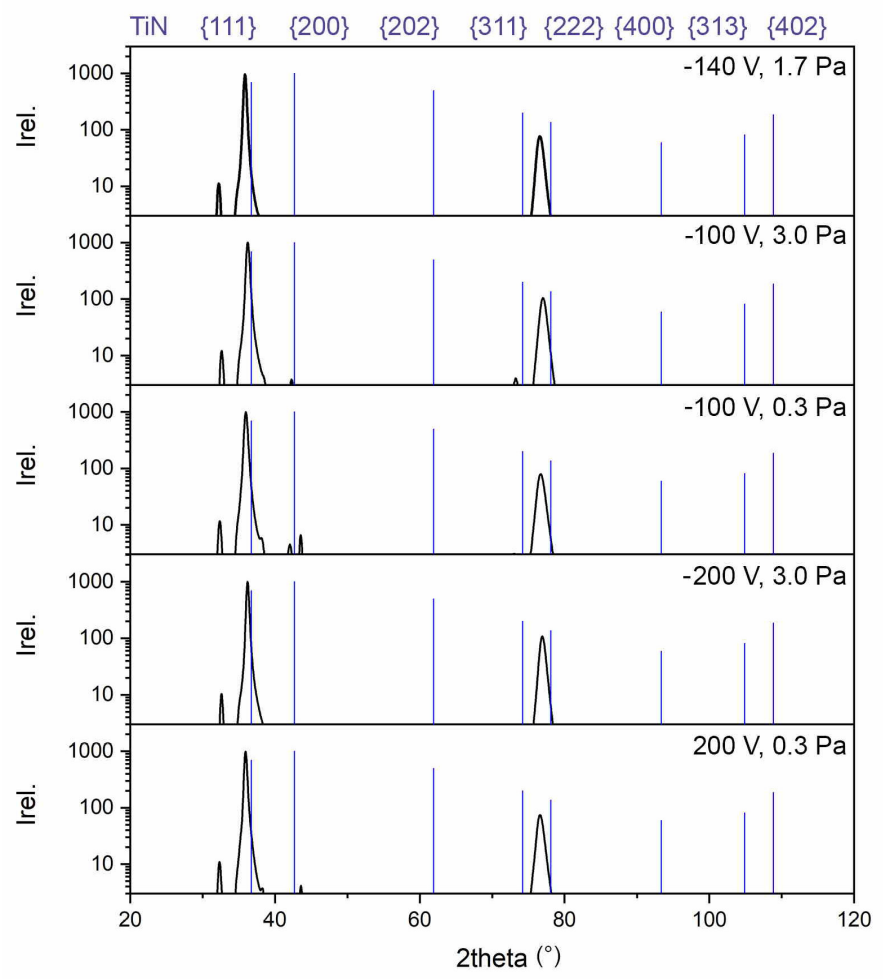

Figure 10. XRD Results.

3.5. Hardness

The hardness of the TiNbN coatings is in the range 13 to 15 GPa and tends to slightly decrease when increasing the negative bias from −100 V to −200 V (see Figure 11). However, in this study, the bias and the pressure do not exhibit a significant impact on the hardness. There is no statistically significant impact of the process parameters on the coating hardness.

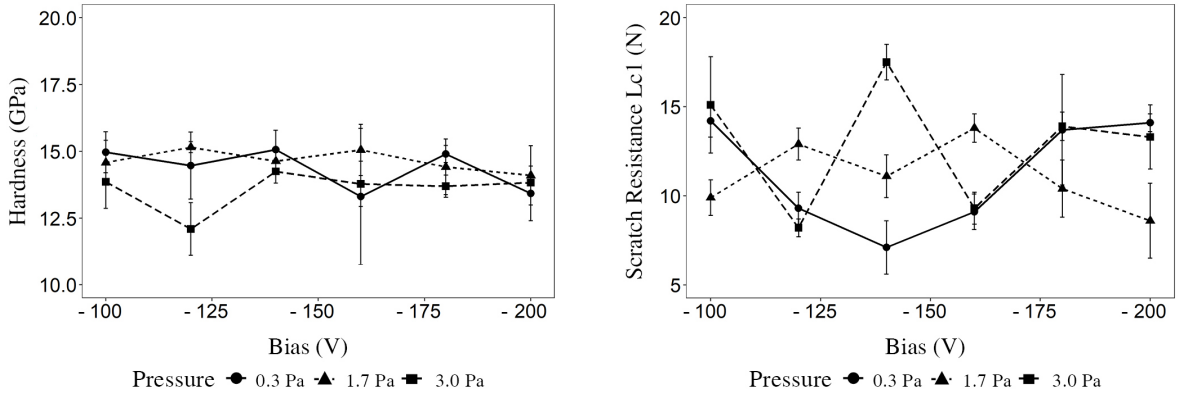

Figure 11. *Cont.*

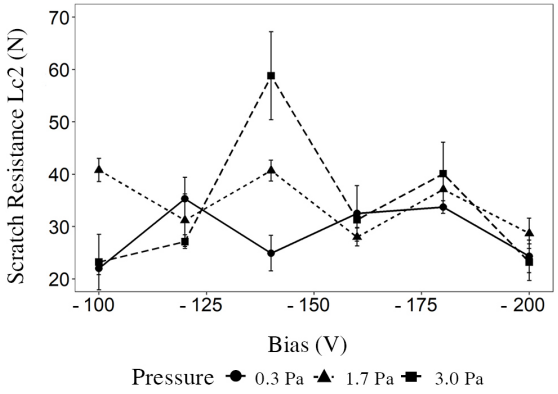

Coefficient	Bias	Pressure	Interaction of Bias & Pressure	Bias^2	Pressure^2
Hardness	0.401	0.067	0.142	0.624	0.057
Lc1	0.940	0.393	0.694	0.492	0.551
Lc2	0.827	0.347	0.968	0.101	0.531
*indicates statistical significance					

Figure 11. Scatter plot of the hardness and scratch resistance (Lc1 and Lc2).

3.6. Scratch Resistance

The scratch resistance of the TiNbN coatings is in the range 10 to 15 N (Lc1) and about 20 to 40 N (Lc2). As an exception, TiNbN shows a maximum scratch resistance of 17.5 N for Lc1 and 58.8 N for Lc2, at 140 V and 3.0 Pa. However, in this study, the bias and nitrogen pressure do not exhibit a significant impact on the scratch resistance (see Figure 11). The process parameters show no statistically significant impact on the scratch resistance.

4. Discussion

4.1. Coating Thickness and Roughness

In this study, the coating thickness was significantly affected by the conditions in the coating process, showing a maximum at high nitrogen pressures and low substrate bias. Additionally, the quadratic proportion of the pressure exhibits a highly significant impact on the coating thickness, indicating the existence of a global maximum that is not covered by the parameter field in this study.

The impact of the pressure on the coating thickness of titanium-based nitride coatings was also examined by Joo et al. [24], who also described a significant increase in coating thickness as a result of an increased nitrogen pressure during the layer application. Keles et al. [40] did not find a significant impact of the pressure on the coating rate. However, this study may not be comparable to the presented data in our study, due to a limited range of pressures. A decrease in the coating thickness, when increasing the substrate bias, is consistent with the findings of Joo et al. [24] and Keles et al. [40] for TiAlN and TiN, respectively.

This effect is also covered by the SZM of Anders [25] and its description of the net deposition rate as a function of the particle energy. The pressure and the substrate bias are known to have a significant impact on the kinetic energy of particles arriving at the substrate surface, by provoking collisions through bombing particles with gas atoms and, thus, decelerating these particles and providing a continuous acceleration to ionised particles on the free path length between the target and the substrate material [18,20,25]. Based on the findings of our study, the reduction in re-sputtering processes is observed in

the multifactorial parameter field, when operating at a relatively high nitrogen pressure and a low substrate bias.

Measurements of the line and surface roughness show relatively low results for coated samples. Additionally, the post-processing step had a significant impact on the measurements of R_a, R_z, R_p and R_v. The nitrogen pressure was the most dominant factor in this study, with respect to line roughness. In addition, the substrate bias was especially significant for samples after the finishing process. Consequently, the line roughness of TiNbN was reduced at high nitrogen pressures and high substrate biases, resulting in a local minimum in the parameter field.

A local minimum at a higher chamber pressure indicates atmosphere-dependent effects at the target surface. A nitridation of the target surface (cathode poisoning) is known to show a significant impact on the spot behaviour of arc sources, affecting the generation of macro particles on films [14,15].

The surface roughness parameters were on a very small scale, independent from the post-processing step. In this study, a significant quadratic proportion of the substrate bias led to a local minimum in the parameter field.

Herbster et al. [8] measured S_a on unloaded TiNbN and TiN surfaces of retrieval implant components, with an S_a between 0.02 and 0.04 µm. Compared to the present study, the test results revealed higher surface roughness parameters. Herbster et al. [8] showed surface roughness values above the samples in this study, prior to the finishing process (as coated). In this study, all measurements were performed on flat, standardised surfaces that provided a feasible measurement area of 0.25 × 0.25 mm. This edge length of the region of interest is more favourable with respect to cut off lengths during roughness measurements and localised effects. Thus, roughness measurements on flat surfaces tend to be more replicable.

With respect to the tribological performance of the coated surfaces and the contact mechanics with polyethylene (PE) counter bodies, R_p and R_v or S_{pk} and S_{vk} tend to be the functional factors to describe the coating characteristics [41]. In general, the roughness of PVD-coated surfaces is slightly higher than the roughness of polished substrate surfaces [7]. The roughness is a result of two effects. R_p and S_{pk} peaks result from the formation of droplets. Pin holes (R_v, S_{vk}) result from droplets released from the surface during the coating process or finishing processes [21].

Shi et al. [34] described a reduction in a global minimum of wear rates in tribosystems when increasing the void volumes of hard layers. Additionally, void volumes show a significant impact on the Stribeck curves of tribosystems, which lead to a shift to hydrodynamic behaviour under the same load conditions [42,43]. Thus, Rv and Svk are likely to have a favourable impact on the tribological behaviour of hard PVD coatings.

4.2. Structure

A more columnar structure of TiNbN, at a higher substrate bias, is comparable to zone 2 of the Thornton model [17–19]. At −100 V, the TiNbN layers exhibit a fine structure with multiple interruptions in the grain growth, which is likely to be in zone T of the Thornton model [17–19].

Thornton described the structure of PVD layers as a function of the substrate temperature and the pressure in the coating chamber [17]. The temperature is a representation of the energy put into the sputtering process, while the pressure is a synonym for the average free path length of emitted ions in the evaporation process. However, instead of the substrate temperature, the bias was analysed in the present study. The bias is more appropriate when representing the energy level of the emitted ions and the acceleration towards the substrate surface during the arc evaporation processes. Thus, substrate bias is likely to show the same effects for arc evaporation processes as the temperature is showing for sputter processes. Consequently, a recrystallisation structure is likely to appear when increasing the substrate bias above −200 V. These findings are in accordance with the SZM

of Anders [25], illustrating the impact of chamber pressure and accelerating bias on the kinetic particle energy.

Contrary to the remaining analyses in this study, the SEM analysis was performed on TiNbN-coated austenitic steel samples. However, due to the surface conditioning prior to exposure to the nitrogen atmosphere, the impact of the substrate on the structure of the TiNbN coatings is subordinate in this analysis. The surface conditioning comprises sputter cleaning and the application of a TiNb-layer.

4.3. Hardness and Scratch Test

In this study, there was no significant impact of the substrate bias or the nitrogen pressure on the hardness. Despite the numerical model, the results of the hardness measurements in this study are consistent with the hardness of TiN coatings that were applied via arc evaporation [40]. However, for TiAlN coatings, a significant impact of bias voltage on the coating hardness was found. Ahlgren et al. [23] and Joo et al. [24] described a range of process bias, with proportional relations between bias and hardness. After reaching the maximum hardness, the proportional section of the function is followed by a plateau of an inversely proportional impact of the bias on the coating hardness. Most likely, the comparatively small range of process bias within this study revealed a section of a plateau when describing the hardness as a function of the process bias.

Eventually, the scratch resistance was not significantly affected by variations of the substrate bias and the nitrogen pressure. Taking the results of the hardness measurements and the XRD analysis into account, the similarity of the critical loads in the scratch tests can be attributed to a comparable microstructure of the TiNbN coatings. Based on the observations in the XRD graph, there seems to be no significant difference in residual stresses in the parameter field in this study.

Compared to data in the literature, the TiNbN coating showed high critical loads in scratch tests [7,8,24]. Herbster et al. [8] performed scratch tests on retrieved total knee arthroplasty components with TiNbN coatings. The critical load (Lc1) was found to be within 2.3–5.1 N on CoCrMo substrates. Lepicka et al. [7] conducted scratch test analyses on polished metal rounds coated with TiN. Lc1 was found to be 2.3 on stainless steel substrates. However, due to the use of an indenter radius of 100 µm, both studies [7,8] varied from DIN EN ISO 20,502 [38] and our study, despite testing equal coating systems (equal substrate and coating thickness). This resulted in a layer failure at lower nominal normal loads, compared to tests under standardised conditions. However, Herbster et al. [8] and the present study could not produce coating delamination (Lc3) within the scratch test. Lepicka et al. [7] induced delamination (Lc3) at 17.1 N.

Joo et al. [24] studied the variation of process parameters on the mechanical properties of TiAlN PVD coatings. The scratch resistance of the coating on steel substrates was not affected by a variation of the bias below −400 V and the critical load was increased significantly at −800 V.

5. Conclusions

Variation of the process parameters of cathodic arc evaporation was used to analyse the impact of the deposition conditions of TiNbN coatings on CoCrMo substrates. The substrate bias was varied between −100 and −200 V. The pressure was varied between 0.3 and 3.0 Pa. The results of the coating thickness, surface morphology, coating structure and mechanical properties can be summarised as follows:

- The nitrogen pressure and the substrate bias of the arc evaporation process show a significant impact on the coating properties of TiNbN.
- The coating thickness is affected by the bias and the pressure, while the nitrogen pressure is the predominant factor.
- The line roughness (Ra, Rz, Rp, Rv) and the surface roughness (Sa, Sz, Spk, Svk) are significantly affected by the bias and the pressure.

- After finishing, the line roughness and surface roughness are reduced to Ra < 0.05 µm and Rp < 0.25 µm. There is no statistically significant impact of the bias and pressure after finishing.
- The structure of the grain growth is affected by the substrate bias, exhibiting a fine grain growth at −100 V (Zone T according to Thornton) and a consistent columnar growth at −200 V (Zone 2 according to Thornton).
- All samples show a cubic TiN-like structure with {111} fibre texture in XRD analysis.
- The hardness and scratch resistance did not show a statistically significant impact of the substrate or pressure within the analysed parameter field.

The findings of the present study help to quantify the effects of a variation of process parameters during the coating process of TiNbN, particularly in the context of existing structure zone models. Furthermore, the presented results can be utilized for tailoring the properties of TiNbN for medical applications with respect to the structure of the grain growth and the surface roughness.

Author Contributions: Conceptualisation, H.D.; methodology, M.P. and S.M.; formal analysis, H.D.; investigation, M.P. and S.M.; resources, A.B.; writing—original draft preparation, H.D.; writing—review and editing, O.K.; visualisation, H.D.; supervision, O.K.; project administration, A.B. All authors have read and agreed to the published version of the manuscript.

Funding: This research received no external funding.

Institutional Review Board Statement: Not applicable.

Informed Consent Statement: Not applicable.

Data Availability Statement: Data sharing is not applicable to this article.

Acknowledgments: The authors would like to acknowledge Sabine Bergmann, Marcus Krawutschke and Daniel Mielke (DOT GmbH) for their valuable support. Further acknowledgement goes to IGMHS GmbH in Rostock, Germany for the preparation of SEM images for this study.

Conflicts of Interest: Henry Dempwolf and Axel Baumann report an employment at DOT GmbH. The other authors declare no conflict of interest.

References

1. Breugem, S.J.M.; Linnartz, J.; Sierevelt, I.; Bruijn, J.D.; Driessen, M.J.M. Evaluation of 1031 primary titanium nitride coated mobile bearing total knee arthroplasties in an orthopedic clinic. *World J. Orthop.* **2017**, *8*, 922–928. [CrossRef] [PubMed]
2. Thomas, P.; Hisgen, P.; Kiefer, H.; Schmerwitz, U.; Ottersbach, A.; Albrecht, D.; Summer, B.; Schinkel, C. Blood cytokine pattern and clinical outcome in knee arthroplasty patients: Comparative analysis 5 years after standard versus "hypoallergenic" surface coated prosthesis implantation. *Acta Orthop.* **2018**, *89*, 646–651. [CrossRef]
3. Fabry, C.; Zietz, C.; Baumann, A.; Bader, R. Wear performance of sequentially cross-linked polyethylene inserts against ion-treated CoCr, TiNbN-coated CoCr and Al2O3 ceramic femoral heads for total hip replacement. *Lubricants* **2015**, *3*, 14–26. [CrossRef]
4. Fabry, C.; Zietz, C.; Baumann, A.; Ehall, R.; Bader, R. High wear resistance of femoral components coated with titanium nitride: A retrieval analysis. *Knee Surg. Sport. Traumatol. Arthrosc.* **2018**, *26*, 2630–2639. [CrossRef] [PubMed]
5. Varnum, C. Outcomes of different bearings in total hip arthroplasty—Implant survival, revision causes, and patient-reported outcome. *Dan. Med. J.* **2017**, *64*, 1–22.
6. Gispert, M.P.; Serro, A.P.; Colaço, R.; Pires, E.; Saramago, B. Wear of ceramic coated metal-on-metal bearings used for hip replacement. *Wear* **2007**, *263*, 1060–1065. [CrossRef]
7. Łępicka, M.; Grądzka-Dahlke, M.; Pieniak, D.; Pasierbiewicz, K.; Kryńska, K.; Niewczas, A. Tribological performance of titanium nitride coatings: A comparative study on TiN-coated stainless steel and titanium alloy. *Wear* **2019**, *422–423*, 68–80. [CrossRef]
8. Herbster, M.; Döring, J.; Nohava, J.; Lohmann, C.H.; Halle, T.; Bertrand, J. Retrieval study of commercially available knee implant coatings TiN, TiNbN and ZrN on TiAl6V4 and CoCr28Mo6. *J. Mech. Behav. Biomed. Mater.* **2020**, *112*, 10403. [CrossRef]
9. Thienpont, E. Titanium niobium nitride knee implants are not inferior to chrome cobalt components for primary total knee arthroplasty. *Arch. Orthop. Trauma Surg.* **2015**, *135*, 1749–1754. [CrossRef]
10. Schroeder, S.; Braun, S.; Mueller, U.; Schroeder, M.; Sonntag, R.; Jaeger, S.; Kretzer, J.P. Polyethylene wear and metal release of TiNbN-coated knee implants. *Wear* **2020**, *458–459*, 203426. [CrossRef]
11. Serro, A.P.; Completo, C.; Colaço, R.; dos Santos, F.; da Silva, C.L.; Cabral, J.M.S.; Araújo, H.; Pires, E.; Saramago, B. A comparative study of titanium nitrides, TiN, TiNbN and TiCN, as coatings for biomedical applications. *Surf. Coatings Technol.* **2009**, *203*, 3701–3707. [CrossRef]

12. Kienle, A.; Graf, N.; Krais, C.; Wilke, H.J. The move-c cervical artificial disc—Design, materials, mechanical safety. *Med. Devices Evid. Res.* **2020**, *13*, 315–324. [CrossRef] [PubMed]
13. Bergschmidt, P.; Bader, R.; Finze, S.; Schulze, C.; Kundt, G.; Mittelmeier, W. Comparative Study of Clinical and Radiological Outcomes of Unconstrained Bicondylar Total Knee Endoprostheses with Anti-allergic Coating. *Open Orthop. J.* **2011**, *5*, 354–360. [CrossRef] [PubMed]
14. Golizadeh, M.; Mendez Martin, F.; Kolozsvári, S.; Anders, A.; Franz, R. Cathode spot behavior in nitrogen and oxygen gaseous atmospheres and concomitant cathode surface modifications. *Surf. Coatings Technol.* **2021**, *421*, 127441. [CrossRef]
15. Oh, K.; Kalanov, D.; Birtel, P.; Anders, A. High-resolution observation of cathodic arc spots in a magnetically steered arc plasma source in low pressure argon, nitrogen, and oxygen atmospheres. *J. Appl. Phys.* **2021**, *130*, 183304. [CrossRef]
16. Oh, K.; Kalanov, D.; Anders, A. High-resolution observation of cathode spots in a magnetically steered vacuum arc plasma source. *Plasma Sources Sci. Technol.* **2021**, *30*, 095005. [CrossRef]
17. Thornton, J.A. Influence of Apparatus Geometry and Deposition Conditions on the Structure and Topography of Thick Sputtered Coatings. *J. Vac. Sci. Technol.* **1974**, *11*, 666–670. [CrossRef]
18. Thornton, J.A. High Rate Thick Film Growth. *Annu. Rev. Mater. Sci.* **1977**, *7*, 239–260. [CrossRef]
19. Thornton, J.A. The microstructure of sputter-deposited coatings. *J. Vac. Sci. Technol. A Vac. Surf. Film.* **1986**, *4*, 3059–3065. [CrossRef]
20. Messier, R.; Giri, A.P.; Roy, R.A. Revised structure zone model for thin film physical structure. *J. Vac. Sci. Technol. A Vac. Surf. Film.* **1984**, *2*, 500–503. [CrossRef]
21. Ali, M.; Hamzah, E.; Qazi, I.A.; Toff, M.R.M. Effect of cathodic arc PVD parameters on roughness of TiN coating on steel substrate. *Curr. Appl. Phys.* **2010**, *10*, 471–474. [CrossRef]
22. Wang, M.; Ma, G.; Liu, X.; Dong, C. Morphology and mechanical properties of TiN coatings prepared with different PVD methods. *Rare Met. Mater. Eng.* **2016**, *45*, 3080–3084. [CrossRef]
23. Ahlgren, M.; Blomqvist, H. Influence of bias variation on residual stress and texture in TiAlN PVD coatings. *Surf. Coatings Technol.* **2005**, *200*, 157–160. [CrossRef]
24. Joo, Y.K.; Zhang, S.H.; Yoon, J.H.; Cho, T.Y. Optimization of the adhesion strength of Arc ion plating TiALN films by the taguchi method. *Materials* **2009**, *2*, 699–709. [CrossRef]
25. Anders, A. A structure zone diagram including plasma-based deposition and ion etching. *Thin Solid Film.* **2010**, *518*, 4087–4090. [CrossRef]
26. Ragone, V.; Canciani, E.; Biffi, C.A.; D'Ambrosi, R.; Sanvito, R.; Dellavia, C.; Galliera, E. CoCrMo alloys ions release behavior by TiNbN coating: An in vitro study. *Biomed. Microdevices* **2019**, *21*, 61. [CrossRef]
27. Bidossi, A.; Bottagisio, M.; De Grandi, R.; De Vecchi, E. Ability of adhesion and biofilm formation of pathogens of periprosthetic joint infections on titanium-niobium nitride (TiNbN) ceramic coatings. *J. Orthop. Surg. Res.* **2020**, *15*, 1–10. [CrossRef]
28. Cicek, H.; Baran, O.; Keles, A.; Totik, Y.; Efeoglu, I. A comparative study of fatigue properties of TiVN and TiNbN thin films deposited on different substrates. *Surf. Coatings Technol.* **2017**, *332*, 296–303. [CrossRef]
29. Arora, J.S. *Additional Topics on Optimum Design*; Elsevier: Amsterdam, The Netherlands, 2017; ISBN 9780128008065.
30. *DIN ISO 5832-12*; Implants for Surgery—Metallic Materials—Part 12: Wrought cobalt-chromium-molybdenum alloy (ISO 5832-12:2007). ISO: Geneva, Switzerland, 2009.
31. *DIN EN ISO 26423*; Fine Ceramics (Advanced Ceramics, Advanced Technical Ceramics)—Determination of Coating Thickness by Crater-Grinding Method (ISO 26423:2009); German version EN ISO 26423:2016. ISO: Geneva, Switzerland, 2016.
32. *DIN EN ISO 4287*; Geometrical Product Specifications (GPS)—Surface Texture: Profile Method—Terms, Definitions and Surface Texture Parameters (ISO 4287:1997 + Cor 1:1998 + Cor 2:2005 + Amd 1:2009); German version EN ISO 4287:1998 + AC:2008 + A1:2009. ISO: Geneva, Switzerland, 2010.
33. *DIN EN ISO 4288*; Geometrical Product Specification (GPS)—Surface Texture: Profile Method—Rules and Procedures for the Assessment of Surface Texture (ISO 4288:1996). German Version EN ISO4288:1997. ISO: Geneva, Switzerland, 1998.
34. Shi, R.; Wang, B.; Yan, Z.; Wang, Z.; Dong, L. Effect of surface topography parameters on friction and wear of random rough surface. *Materials* **2019**, *12*, 2762. [CrossRef]
35. Chateigner, D.; Chen, X.; Cirriotti, M.; Downs, R.T.; Gražulis, S.; Kaminsky, W.; Le Bail, A.; Lutterotti, L.; Matsushita, Y.; Merkys, A.; et al. Crystallography Open Database. Available online: https://www.crystallography.net/cod/ (accessed on 19 March 2022).
36. Brandenburg, H.P.K. Crystal Impact. Available online: https://www.crystalimpact.com/match/ (accessed on 19 March 2022).
37. *DIN EN ISO 14577-4*; Metallic Materials—Instrumented Indentation Test for Hardness and Materials Parameters—Part 4: Test Method for Metallic and Non-Metallic Coatings. ISO: Geneva, Switzerland, 2016.
38. *DIN EN ISO 20502*; Fine Ceramics (Advanced Ceramics, Advanced Technical Ceramics)—Determination of Adhesion of Ceramic Coatings by Scratch Testing (ISO 20502:2005 including Cor 1:2009); German version EN ISO 20502:2016. ISO: Geneva, Switzerland, 2016.
39. Lenth, R.V. Response-surface methods in R, using RSM. *J. Stat. Softw.* **2009**, *32*, 1–17. [CrossRef]
40. Keles, O.; Taptik, Y.; Eryilmaz, O.L.; Urgen, M.; Çakir, A.F. Optimization of arc-PVD TiN coating process parameters by Taguchi technique. *Qual. Eng.* **1999**, *12*, 29–36. [CrossRef]

41. Popov, V.L. Method of reduction of dimensionality in contact and friction mechanics: A linkage between micro and macro scales. *Friction* **2013**, *1*, 41–62. [CrossRef]
42. Wang, Y.; Wang, Q.J.; Lin, C.; Shi, F. Development of a set of stribeck curves for conformal contacts of rough surfaces. *Tribol. Trans.* **2006**, *49*, 526–535. [CrossRef]
43. Bachchhav, B.; Bagchi, H. Effect of surface roughness on friction and lubrication regimes. *Mater. Today Proc.* **2020**, *38*, 169–173. [CrossRef]